Organic Peroxyl Radical Photolysis in the Near-Infrared: Effects on Tropospheric Chemistry

Gregory J. Frost*

Aeronomy Laboratory, National Oceanic and Atmospheric Administration, and Cooperative Institute for Research in Environmental Sciences, University of Colorado, Boulder, Colorado

G. Barney Ellison and Veronica Vaida*

Department of Chemistry & Biochemistry, University of Colorado, Boulder, Colorado

Received: May 27, 1999; In Final Form: July 30, 1999

We investigate the effects of near-infrared photolysis of organic peroxyl radicals (RO_2) on tropospheric chemistry. We propose that the excitation of an RO_2 to its lowest excited electronic state with near-infrared (near-IR) light is followed by intramolecular reactions that produce hydroxyl (OH) or hydroperoxyl (HO_2) radicals. Spectra to this low-lying state have recently been obtained, but absorption cross sections for this electronic transition and yields of the resulting photoproducts have not been directly measured. We suggest a limiting range of cross sections from estimates for the same transition in HO_2 and by comparison to other allowed electronic transitions. On the basis of a thermochemical assessment, we propose that OH and an aldehyde are the principal photoproducts of near-IR photolysis of RO_2. These photolysis reactions are included in a model of the troposphere with a standard photochemical mechanism and conditions appropriate to remote, rural, and urban locations. Inclusion of RO_2 photolysis has a small effect on any of the major tropospheric chemical constituents if lower limit estimates of the absorption cross sections are used. Midrange or upper limit cross section estimates result in significant departures from the currently accepted photochemical scheme. These studies provide a clear need for further measurements of RO_2 absorption cross sections and photoproduct yields, which are the principal uncertainties.

1. Introduction

Peroxyl radicals play a central role in the chemistry of the troposphere. Because of their close coupling to the hydroxyl radical OH, they are involved in photochemical smog production, acid formation and precipitation, and the control of emitted trace species such as carbon monoxide and volatile organic compounds (VOCs).[1−4] Organic peroxyl radicals (R−O−O or RO_2, where R is a carbon-containing chain) are generated in the atmospheric oxidation of biogenic and anthropogenic VOCs. These peroxyl radicals are intimately connected to various tropospheric chemical cycles through reactions involving the radical families HO_x ($OH + HO_2$) and NO_x ($NO + NO_2$). By oxidizing NO to NO_2, RO_2 are key reactants in the photochemical production of tropospheric ozone.

We investigate the relationship between atmospheric radicals and radiation by proposing a new photochemical reaction for organic peroxyl radicals. This novel photochemistry of RO_2 requires reaction on the lowest electronic state of A′ symmetry as described by Clifford et al.[5] This excited state can be pumped by near-infrared (near-IR) solar radiation (5500 to 9000 cm^{-1}). The excited peroxyl radicals can then form cyclic structures which facilitate intramolecular reactions, with possible products including either an aldehyde and OH or an alkene and HO_2.

This photochemical reaction channel has the potential to affect the tropospheric concentrations and diurnal distribution of RO_2, HO_x, NO_x, O_3, and other compounds. A photochemical box model allowed us to explore the tropospheric consequences of the near-IR photolysis of peroxyl radicals. The model results underscore the complexity of tropospheric chemistry demonstrated in the three situations investigated, including a remote site with low VOC and NO_x levels, a rural location with high [VOC] and moderate [NO_x], and an urban environment with high [VOC] and [NO_x]. It has been pointed out[6] that the nonlinear dependence between radical families makes model predictions of local HO_x concentrations and O_3 production challenging. The proposed addition of RO_2 near-IR photolysis to the currently understood photochemical mechanism amplifies these effects. Our model results illustrate the nonlinear coupling between solar radiation and radical chemistry as well as that between the different radical families in the troposphere. Recent atmospheric measurements of radical levels[7−11] have begun to probe these complex relationships. Our model calculations suggest the sensitivities needed for observation of the proposed RO_2 photochemistry.

2. Proposed RO_2 Photolysis Channels in the Troposphere

The proposed tropospheric photochemical reactions involve near-IR solar pumping of RO_2 radicals to an excited electronic state in which the radical undergoes rearrangement and decomposition. The chemistry and spectroscopy of alkylperoxyl radicals has been studied recently.[1,5] All RO_2 radicals have a low-lying electronic state that is within 1 eV of the ground state. In particular the ground state of CH_3O_2 is $\tilde{X}^2A''$ and the first excited state is $\tilde{A}^2A'$ with $T_e = 7375 \pm 2$ cm^{-1} (0.9144 ± 0.0002 eV, 1.3559 μm).[12,13]

Tropospheric oxidation of methane produces CH_3 which rapidly combines with oxygen to produce CH_3O_2 $\tilde{X}^2A''$.[14] Solar pumping of the methylperoxyl radical at 7375 cm^{-1} will

* To whom correspondence may be addressed.

10.1021/jp9917547 CCC: $18.00
Published on Web 09/08/1999

populate the $\tilde{A}^2A'$ state of CH_3O_2, which will decompose to formaldehyde and OH.

$$CH_3O_2\ \tilde{X}^2A'' + h\nu_{1.36\mu m} \rightarrow [CH_3O_2\ \tilde{A}^2A']^* \rightarrow HCH(O) + OH \quad (R1)$$

The decomposition of $\tilde{A}^2A'$ CH_3O_2 in R1 is exothermic by 40.2 $\pm$ 0.8 kcal mol^{-1}.[5] This (1,4) fragmentation of $\tilde{A}^2A'$ CH_3O_2 to produce HCH(O) and rotationally excited OH can be described by the GVB diagrams.[15]

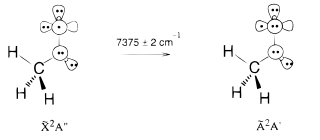

(R2)

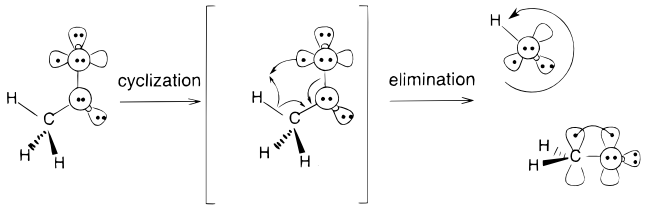

$\tilde{A}^2A'$ (R3)

The (1,4) cyclization barrier, estimated by Clifford et al.[5] to be about 15 kcal mol^{-1} in the $\tilde{A}^2A'$ state, appears to be a little over 20 kcal mol^{-1} in light of recent theoretical calculations.[16] Excited vibrational levels in the $\tilde{A}^2A'$ state would have enough energy to overcome such barriers.

In addition to (1,4) fragmentations which generate aldehydes and OH radicals, more complex alkylperoxyl radicals can undergo (1,5) decompositions to yield alkenes and the hydroperoxyl radical.[1,5]

$$CH_2CH_2O_2\ \tilde{X}^2A'' + h\nu_{1.32\ \mu m} \rightarrow [RCH_2CH_2O_2\ \tilde{A}^2A']^* \rightarrow RCH{=}CH_2 + HO_2 \quad (R4)$$

The activation energy required to close a five-member activated complex is expected to be small.[5] Both the (1,4) and (1,5) rearrangements feature an internal abstraction of a H atom but both are unlikely to occur from the ground states of the alkylperoxyl radicals, $\tilde{X}^2A''$, because of poor orbital overlap. In contrast, a more "reactive" configuration of RO_2 will be $\tilde{A}^2A'$.

The purpose of this paper is to demonstrate some of the atmospheric implications of RO_2 near-IR photolysis, which requires knowledge of the rates of the two possible reaction channels illustrated by R1 and R4. Theoretical and experimental studies of thermal reactions of alkyl radicals and O_2, in which alkylperoxyl radicals are intermediates, suggest that the various products result from coupling between two potential energy surfaces of $^2A''$ and $^2A'$ symmetry.[17−22] There are still many unanswered questions about the reactivity on the excited $^2A'$ surface, and direct experimental studies will be needed to resolve uncertainties in the photochemistry we propose here. In the absence of the necessary rates for this excited state chemistry, we have done the following. We first describe the known tropospheric chemistry of peroxyl radicals in section 3. In section 4 we outline thermochemical calculations of the proposed reaction channels for various RO_2 species and eliminate photoproducts not thermodynamically accessible by near-IR excitation. Absorption cross sections and quantum yields for the two possible reaction channels have yet to be determined experimentally. In section 5 we therefore estimate the rate of photolysis of peroxyl radicals in the near-IR. We assume that the overall rate is limited by the near-IR excitation and that the thermodynamically allowed excited state photoproducts will subsequently form with unit efficiency.

TABLE 1: Key Tropospheric Photochemical Reactions

no. of reaction	reaction
R5	$O_3 + h\nu \rightarrow O(^1D) + O_2$
R6[a]	$O(^1D) + M \rightarrow O(^3P) + M$
R7	$O(^1D) + H_2O \rightarrow OH + OH$
R8	$OH + H_2 \rightarrow H_2O + H$
R9	$OH + CO \rightarrow CO_2 + H$
R10	$H + O_2 + M \rightarrow HO_2 + M$
R11	$OH + CH_4 \rightarrow CH_3 + H_2O$
R12	$CH_3 + O_2 + M \rightarrow CH_3O_2 + M$
R13[b]	$RH + OH \rightarrow R + H_2O$
R14	$R + O_2 + M \rightarrow RO_2 + M$
R15	$R{=}R' + OH + M \rightarrow HORR' + M$
R16	$HORR' + O_2 + M \rightarrow HORR'O_2 + M$
R17	$HO_2 + NO \rightarrow OH + NO_2$
R18	$HO_2 + O3 \rightarrow OH + 2O_2$
R19	$HO_2 + HO_2 \rightarrow H_2O_2 + O_2$
R20	$CH_3O_2 + NO \rightarrow CH_3O + NO_2$
R21	$CH_3O_2 + HO_2 \rightarrow CH_3OOH + O_2$
R22a	$CH_3O_2 + CH_3O_2 \rightarrow 2CH_3O + O_2$
R22b	$CH_3O_2 + CH_3O_2 \rightarrow HCH(O) + CH_3OH + O_2$
R23	$CH_3O + O_2 \rightarrow HCH(O) + HO_2$
R24	$RH_2CO_2 + NO \rightarrow RH_2CO + NO_2$
R25	$RH_2CO + O_2 \rightarrow RCH(O) + HO_2$
R26	$RO_2 + HO_2 \rightarrow ROOH + O_2$
R27	$H_2O_2 + h\nu \rightarrow OH + OH$
R28	$CH_3OOH + h\nu \rightarrow CH_3O + OH$
R29	$RH_2COOH + h\nu \rightarrow RH_2CO + OH$
R30	$OH + H_2O_2 \rightarrow H_2O + HO_2$
R31a	$OH + CH_3OOH \rightarrow CH_3O_2 + H_2O$
R31b	$OH + CH_3OOH \rightarrow HCH(O) + OH + H_2O$
R32	$OH + ROOH \rightarrow RO_2 + H_2O$
R33a	$HCH(O) + h\nu \rightarrow H_2 + CO$
R33b	$HCH(O) + h\nu \rightarrow HCO + H$
R34	$RCH(O) + h\nu \rightarrow R + HCO$
R35	$HCO + O_2 \rightarrow CO + HO_2$
R36	$OH + HCH(O) \rightarrow HCO + H_2O$
R37	$OH + RCH(O) \rightarrow RC(O) + H_2O$
R38	$RC(O) + O_2 + M \rightarrow RC(O)O_2 + M$
R39	$RC(O)O_2 + NO_2 + M \rightarrow RC(O)O_2NO_2 + M$
R40	$OH + HO_2 \rightarrow H_2O + O_2$
R41	$OH + NO_2 + M \rightarrow HNO_3 + M$
R42	$NO_2 + h\nu \rightarrow NO + O(^3P)$
R43	$O(^3P) + O_2 + M \rightarrow O_3 + M$

[a] M = any air molecule, predominantly N_2 and O_2. [b] R = organic chain.

3. Current Tropospheric RO_2 Photochemical Mechanism

To establish how the proposed peroxyl radical photolysis will affect tropospheric chemistry, we must consider the current understanding of peroxyl radical sources and sinks and their connection to other chemical families.[1,4] Table 1 is a list of the key chemical reactions in the troposphere, which we briefly outline here.

This chemistry is initiated by the photolysis of ozone at wavelengths shorter than about 340 nm (R5). Any $O(^1D)$ from R5 not quenched in R6 can react with H_2O to produce OH (R7). Peroxyl radicals are generated by OH reactions with reduced species such as H_2, CO, alkanes, and alkenes (R8, R9, R11, R13, R15) followed by barrierless reactions of H or R radicals with O_2 (R10, R12, R14, R16). HO_2 is destroyed by reactions with NO (R17) and O_3 (R18), which recycle the original OH, and by reacting with another HO_2 to produce hydrogen peroxide

(R19). The main losses of organic peroxyl radicals are reactions with NO to produce an aldehyde and HO_2 (R20 followed by R23, R24 followed by R25) and with HO_2 to form a peroxide (R21, R26). $RO_2 + RO_2$ reactions, such as R22, are generally less important RO_2 loss channels.

The products of these RO_2 loss reactions can themselves be secondary radical sources. H_2O_2 photolysis produces OH radicals (R27), while photolysis of the organic peroxides produces OH, HO_2, and an aldehyde (R28, 29). OH oxidation of peroxides (R30, 31, 32) liberates the parent RO_2 but not the parent HO_2. Photolysis of aldehydes generally produces HO_2 and an RO_2 with one less carbon than the parent (R33b followed by R35 and R10, R34 followed by R35 and R14), though formaldehyde photolysis also has an important channel with only molecular products (R33a). Reaction of aldehydes with OH produces CO and HO_2 in the case of HCH(O) (R36 followed by R35) and an acyl peroxy radical in the case of larger aldehydes (R37 followed by R38). Acyl peroxy radicals (such as $CH_3C(O)O_2$, peroxy acetyl (PA)) can combine with NO_2 to produce peroxy acyl nitrates (e.g., $CH_3C(O)O_2NO_2$, peroxy acetyl nitrate (PAN)). At higher temperatures these nitrates rapidly undergo thermal decomposition, but at lower temperatures they represent a reservoir for both radicals and NO_2 (R39). Other radical termination processes include peroxide formation (R19, R21, R26) followed by OH reaction (R30, R31, R32), R40, R41, and heterogeneous losses of peroxides and aldehydes.

An important consequence of the radical chemistry described above is ozone formation. NO_2 produced from reactions of HO_2 or RO_2 with NO (R17, R20, and R24) is rapidly photolyzed in the visible (R42), and the resulting $O(^3P)$ combines with O_2 to form O_3 (R43). This is the predominant photochemical source of tropospheric ozone and is generally limited by the rates of the $HO_2 + NO$ (R17) and $RO_2 + NO$ (R20, R24) reactions. When [NO] is greater than a few parts per trillion by volume (pptv), ozone production is faster than its losses (R5 followed by R7, R18).

4. Thermochemistry of RO_2 Near-IR Photolysis

We carried out thermochemical calculations for various RO_2 species to understand the photoproducts resulting from near-IR excitation from the ground $\tilde{X}\ ^2A''$ state to the excited $\tilde{A}\ ^2A'$ state (Table 2). The enthalpy of reaction ($\Delta_{rxn}H_{298}$) for this process is the sum of the enthalpies of formation (Δ_fH_{298}) for the photoproducts minus the sum of Δ_fH_{298} for $RO_2(\tilde{X})$ and the near-IR photon energy. We assumed the photon energy was just enough to excite RO_2 from its lowest rovibrational level in the $\tilde{X}$ state to the lowest rovibrational level in the $\tilde{A}$ state.[12] A particular photolysis channel is energetically accessible in the near-IR if $\Delta_{rxn}H_{298} \leq 0$. This approach allows us to narrow down the new reactions we must include in the photochemical scheme, though it does not indicate the rate or branching ratios of the photoproduct channels.

Table 2 summarizes the calculations for HO_2, CH_3O_2, $CH_3CH_2O_2$, $CH_3C(O)O_2$, $HOCH_2CH_2O_2$, and $HOCH_2C(O)O_2$, which are the peroxyl radicals produced from the oxidation of CO, methane, ethane, and ethene. We did not consider RO_2 derived from VOCs with more than 2 carbon atoms given the lack of information about their spectra and thermochemistry. For completeness we show other possible reaction products in Table 2 besides those of the (1,4) and (1,5) rearrangement, though none of these other channels are thermodynamically allowed for a near-IR excitation. HO_2 cannot be photolyzed in the near-IR, since both channels are substantially endothermic; an excitation to the ultraviolet $\tilde{B}\ ^2A''$ state is required. CH_3O_2 near-IR photolysis results in only one allowed product channel: OH + formaldehyde. For $CH_3CH_2O_2$, an analogous set of products (OH and acetaldehyde) is obtained with high exothermicity, while the HO_2 + ethene channel is thermoneutral within the uncertainties of the thermochemical data. Peroxyl acetyl radical, $CH_3C(O)O_2$, cannot photolyze in the near-IR. All investigated photolysis channels of $HOCH_2CH_2O_2$ are exothermic with near-IR excitation. The only exothermic route for $HOCH_2C(O)O_2$ photolysis produces HCH(O), CO_2, and OH. These calculations relied on Δ_fH_{298} values for $HOCH_2CH_2O_2$, $HOCH_2CH(O)$, and $HOCH_2C(O)O_2$ which have not been directly measured. The values used here were estimated from model calculations and from enthalpies for analogous species and reactions using Hess' law (see Table 2 footnotes). Experimental measurements of these enthalpies would be useful.

These thermochemical calculations suggest that the principal near-IR photolytic channel for organic peroxyl radicals produces OH and an aldehyde. Consequently, out of all of the possible near-IR photolysis reactions, four were added to the model chemical scheme:

methane oxidation

$$CH_3O_2 + h\nu \rightarrow HCH(O) + OH \qquad (R44)$$

ethane oxidation

$$CH_3CH_2O_2 + h\nu \rightarrow CH_3CH(O) + OH \qquad (R45)$$

ethene oxidation

$$HOCH_2CH_2O_2 + h\nu \rightarrow HOCH_2CH(O) + OH \qquad (R46)$$

$$HOCH_2C(O)O_2 + h\nu \rightarrow HCH(O) + CO_2 + OH \qquad (R47)$$

In the case of $HOCH_2CH_2O_2$ photolysis (R46), it seems reasonable to conclude that the most exothermic channel, $HOCH_2CH(O) + OH$, will predominate. R46 produces hydroxyacetaldehyde (HAC), $HOCH_2CH(O)$, which is not otherwise formed in the chemical mechanism when oxidation of VOCs with two or fewer carbon atoms is considered. Its fate is either photolysis (R34) or reaction with OH (R37). The $HOCH_2$ radical formed from photolysis rapidly reacts with O_2 to form HCH(O) and HO_2. R37 followed by R38 leads to $HOCH_2C(O)O_2$ (hydroxyl peroxy acetyl, or HPA), which also does not appear in the reference chemical mechanism. As with other acyl peroxyl radicals, R35 will produce $HOCH_2C(O)O_2NO_2$ (HPAN), a third species only appearing in the mechanism when RO_2 photolysis is included.

5. RO_2 Near-IR Photolysis Rate Coefficients

The photolysis rate coefficient, or j value, of a species (units of s^{-1}) is given by

$$j = \int \sigma(\lambda)\phi(\lambda)I(\lambda)d\lambda \qquad (1)$$

where λ is wavelength, $\sigma(\lambda)$ is the absorption cross section (units of cm^2), $\phi(\lambda)$ is the photolysis quantum yield, and $I(\lambda)$ is the actinic (solar) flux (units of photons $cm^{-2}\ s^{-1}$).[4] In the following calculations we assumed $\phi(\lambda)$ was 1, and $I(\lambda)$ was obtained from the Madronich radiative transfer model.[23]

Cross sections for the near-IR transitions have not been directly measured. Hunziker and Wendt[24] estimated that the σ_{max} of the $HO_2\ \tilde{A}\ ^2A' \leftarrow \tilde{X}\ ^2A''$ (0,0) transition (where (n,m) indicates the excitation is from the lower electronic state with

TABLE 2: Thermochemistry of Peroxyl Radical Near-IR Photolysis Reactions[a]

RO_2 and Δ_fH_{298}	+	photon[b]	→	products and Δ_fH_{298}						$\Delta_{rxn}H_{298}$
HO_2	+	$h\nu$	→	H	+	O_2				
2.8		20.1		52.1		0				29.2
			→	OH	+	$O(^3P)$				
				9.3		59.57				45.97
CH_3O_2	+	$h\nu$	→	HCH(O)	+	OH				
4		21.1		−26		9.3				−41.8
			→	CH_3	+	O_2				
				35		0				
			→	CH_3O	+	$O(^3P)$				
				4		59.57				38.47
			→	CH_2	+	HO_2				
				93		2.8				70.7
$CH_3CH_2O_2$	+	$h\nu$	→	$CH_3CH(O)$	+	OH				
−6		21.7		−39.7		9.3				−46.1
			→	$H_2C{=}CH_2$	+	HO_2				
				12.45		2.8				−0.45
			→	CH_3CH_2	+	O_2				
				28.4		0				12.7
			→	CH_3CH_2O	+	$O(^3P)$				
				−4.1		59.57				39.77
$CH_3C(O)O_2$	+	$h\nu$	→	$H_2C{=}C(O)$	+	HO_2				
−41		15.9		−11		2.8				16.9
			→	$CH_3C(O)$	+	O_2				
				−2.4		0				22.7
			→	CH_3	+	CO_2	+	$O(^3P)$		
				35		−94.07		59.57		25.6
			→	CH_2	+	CO_2	+	OH		
				93		−94.07		9.3		33.33
			→	CH_3	+	CO	+	O_2		
				35		−26.42		0		33.68
			→	$CH_3C(O)O$	+	$O(^3P)$				
				−49.6		59.57				35.07
			→	CH_2	+	CO	+	HO_2		
				93		−26.42		2.8		94.48
$HOCH_2CH_2O_2$	+	$h\nu$	→	$HOCH_2CH(O)$	+	OH				
−42.4[c]		21.7[d]		−86.7[e]		9.3				−56.7
			→	HCH(O)	+	HCH(O)	+	OH		
				−26		−26		9.3		−22
			→	$HOCH{=}CH_2$	+	HO_2				
				−30[f]		2.8				−6.5
$HOCH_2C(O)O_2$	+	$h\nu$	→	HCH(O)	+	CO_2	+	OH		
−88[g]		15.9[h]		−26		−94.07		9.3		−38.67
			→	HCH(O)	+	CO	+	HO_2		
				−26		−26.42		2.8		22.48

[a] All enthalpies given in kcal mol^{-1}. Δ_fH_{298} taken from DeMore et al.[28] except where noted. [b] For excitation of the given RO_2 from the ground rovibrational level of the $\tilde{X}$ state to the ground rovibrational level of the $\tilde{A}$ state.[12] [c] Derived by assuming that $\Delta_{rxn}H_{298}$ of $HOCH_2CH_2O_2 \rightarrow HOCH_2CH_2 + O_2$ equals $\Delta_{rxn}H_{298}$ of $CH_3CH_2O_2 \rightarrow CH_3CH_2 + O_2$ (34.4 kcal mol^{-1}) and then subtracting this $\Delta_{rxn}H_{298}$ from the sum of Δ_fH_{298} for $HOCH_2CH_2$ and O_2. [d] $HOCH_2CH_2O_2$ assumed to have same spectrum as $CH_3CH_2O_2$. [e] From semiempirical calculations of Chen et al.[32] [f] Average of Δ_fH_{298} from Turecek and Havlas[33] and Holmes and Lossing.[34] [g] We assumed that $\Delta_{rxn}H_{298}[HOCH_2C(O)O_2 \rightarrow OH + CH_2C(O)O_2] = \Delta_{rxn}H_{298}[HOCH_2CH(O) \rightarrow OH + CH_2CH(O)]$ and $\Delta_{rxn}H_{298}[CH_3C(O)O_2 \rightarrow H + CH_2C(O)O_2] = \Delta_{rxn}H_{298}[CH_3CH(O) \rightarrow H + CH_2CH(O)]$. We calculated $\Delta_{rxn}H_{298}$ for the aldehyde reactions using $\Delta_{rxn}H_{298}[CH_2CH(O)]$ from Rossi and Golden.[35] Then $\Delta_fH_{298}[HOCH_2C(O)O_2] = \Delta_{rxn}H_{298}[CH_3C(O)O_2 \rightarrow H + CH_2C(O)O_2] - \Delta_{rxn}H_{298}[HOCH_2C(O)O_2 \rightarrow OH + CH_2C(O)O_2] - \Delta_fH_{298}[H] + \Delta_fH_{298}[CH_3C(O)O_2] + \Delta_fH_{298}[OH]$. [h] $HOCH_2C(O)O_2$ assumed to have same spectrum as $CH_3C(O)O_2$.

m quanta in the active vibrational mode to the upper electronic state with *n* quanta in this vibrational mode) was on the order of 10 L mol^{-1} cm^{-1} (equivalent to 3.8×10^{-20} cm^2) by comparison of the intensities of this transition with those of the ultraviolet $\tilde{B}\ ^2A'' \leftarrow \tilde{X}\ ^2A''$ transition. From the spectra in Hunziker and Wendt[12] we see that the HO_2 $\tilde{A} \leftarrow \tilde{X}(1,0)$ σ_{max} is about twice that of $\sigma_{max}(0,0)$. The strongest transition in the $\tilde{A} \leftarrow \tilde{X}$ spectra of all other RO_2 in Hunziker and Wendt[12] is the (0,0). We made the assumption that the $\sigma_{max}(0,0)$ for all other RO_2 are approximately the same as $\sigma_{max}(1,0)$ for HO_2, or about 8×10^{-20} cm^2. The Hunziker and Wendt[12] spectra were then used to scale the RO_2 $\sigma_{max}(n,0)$ where $n > 0$. We also assumed that the $HOC_2H_4O_2$ cross sections were the same as those of $C_2H_5O_2$ and that the cross sections of $HOCH_2C(O)O_2$ were equal to those of $CH_3C(O)O_2$, since the spectra of the hydroxylated RO_2 species have not been measured.

The *j* values could then be derived by using eq 1. The version of the Madronich radiative transfer model[23] we used did not give accurate actinic flux predictions in the near-IR because the absorptions due to H_2O, CO_2, and O_4 were not included. We obtained the actinic flux for overhead sun including these absorptions from another radiative transfer model.[25] Using this actinic flux, the above estimated cross sections, and an assumed quantum yield of 1, we derived the following for overhead sum:

$$j(CH_3O_2) = 2.5 \times 10^{-4}\ s^{-1} \approx 10^{-3}\, j(NO_3) \quad (2)$$

$$j(C_2H_5O_2) = 6 \times 10^{-4}\ s^{-1} \approx 2.4 \times 10^{-3}\, j(NO_3) \quad (3)$$

$$j(CH_3COO_2) = 5 \times 10^{-4}\ s^{-1} \approx 2 \times 10^{-3}\, j(NO_3) \quad (4)$$

Actinic flux in the wavelength regions of NO_3 and RO_2 absorptions should vary in approximately the same manner with solar zenith angle (angle of Sun from normal with respect to Earth's surface). We therefore used the zenith angle dependence of $j(NO_3)$ as a surrogate for that of $j(RO_2)$. We scaled $j(NO_3)$

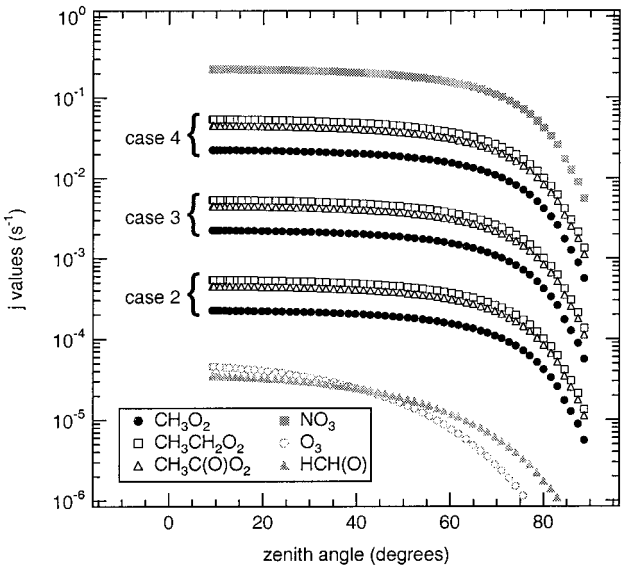

Figure 1. Estimated *j* values for RO_2 species whose near-IR spectra have been measured, as a function of zenith angle at the rural location. *J* values of NO_3, $O_3 \rightarrow O(^1D)$, and the HCH(O) radical channel are also shown for comparison. Box model cases 2, 3, and 4 included RO_2 photolysis with the indicated *j* values.

calculated by the Madronich radiative transfer model[23] according to eqs 2−4 to obtain each $j(RO_2)$ as a function of zenith angle.

The cross sections estimated above for the RO_2 $\tilde{A} \leftarrow \tilde{X}$ spectra are rather small for allowed electronic molecular transitions, which can exceed 10^{-17} cm^2.[26] Ultraviolet transitions to the RO_2 $\tilde{B}\ ^2A''$ state have peak cross sections in the range[1] of 3×10^{-18} to 1×10^{-17} cm^2, which is 40−125 times larger than the Hunziker and Wendt[12] estimate for the $\tilde{A} \leftarrow \tilde{X}$ transition. We cannot assume the cross sections of the $\tilde{A} \leftarrow \tilde{X}$ and $\tilde{B} \leftarrow \tilde{X}$ transitions will be the same because the two excited states have different symmetries. However, it is likely that the above cross section estimates for the $\tilde{A} \leftarrow \tilde{X}$ transition represent a lower limit to the true values and therefore may cause us to underestimate the near-IR RO_2 photolysis rates. In the box model runs described below, we investigated the sensitivity to RO_2 photolysis by increasing $\sigma(\lambda)$ to span the range for allowed electronic transitions. Four different cases were examined for the RO_2 near-IR cross sections:

$$j(RO_2) = 0 \text{ (no } RO_2 \text{ photolysis included)} \quad (1)$$

$$\sigma_{max}[RO_2\ \tilde{A} \leftarrow \tilde{X}(0,0)\ ] = 8 \times 10^{-20}\ \text{cm}^2 \text{ and } j(RO_2) \approx 10^{-3}\, j(NO_3) \quad (2)$$

$$\sigma_{max}[RO_2\ \tilde{A} \leftarrow \tilde{X}(0,0)] = 8 \times 10^{-19}\ \text{cm}^2 \text{ and } j(RO_2) \approx 10^{-2}\, j(NO_3) \quad (3)$$

$$\sigma_{max}[RO_2\ \tilde{A} \leftarrow \tilde{X}(0,0)] = 8 \times 10^{-18}\ \text{cm}^2 \text{ and } j(RO_2) \approx 10^{-1}\, j(NO_3) \quad (4)$$

The RO_2 *j* values in case 2 are probably a lower limit and those of case 4, an upper limit, to the true values. The *j* values for the above cases as a function of zenith angle at one of the model locations are shown in Figure 1.

6. Photochemical Box Model Description

The photochemical box model was similar to one described previously[27] with a few modifications. Each chemical species in the model with the exception of those discussed below was allowed to vary with time. The time-dependent concentrations of shorter lived species (OH, RO_2, and most of the reactive nitrogen compounds) were assumed to be controlled by only photochemical reactions. The levels of longer lived species can be significantly affected by photochemistry and physical or transport processes such as emission from the surface, surface deposition, and advection. The time-dependent concentrations of longer lived compounds were therefore calculated from the photochemistry but were additionally constrained by a "virtual" source or sink term to reach a specified value at local noon. These "virtual" sources and sinks were expressed simply as additional first-order production and loss rates in the chemical continuity equations. There was no explicit atmospheric transport included in the box model. Rate constants were obtained from DeMore et al.[28] *J* values were precalculated for a fixed set of zenith angles and for various locations using the Madronich radiative transfer model[23] and then interpolated by the box model for the appropriate zenith angle at each time step. We kept $[H_2O]$, $[CH_4]$, [M], temperature, pressure and altitude fixed at all times. To limit the number of new RO_2 photolysis reactions carried in the mechanism, we lumped alkanes with two or more carbons as "ethane" and alkenes as "ethene":

$$[\text{"ethane"}] = \frac{k_{OH+C_2H_6}[C_2H_6] + k_{OH+C_3H_8}[C_3H_8] + ...}{k_{OH+C_2H_6}} \quad (5)$$

$$[\text{"ethene"}] = \frac{k_{OH+C_2H_4}[C_2H_6] + k_{OH+C_3H_6}[C_3H_8] + ...}{k_{OH+C_2H_4}} \quad (6)$$

The chemical mechanism included reactions R5−R43 for VOCs containing one to two carbon atoms and, in cases two to four, the RO_2 near-IR photolysis reactions R44−R47.

We considered three sets of chemical environments, chosen to represent remote, rural, and urban locations (see Table 3). We chose these locations in order to understand the effects of the RO_2 photolysis channels for different NO_x and VOC levels. As mentioned above, four cases were run at each location (start time was just before local noon). Integration was carried out until a constant diurnal cycle was achieved in all time-varying concentrations. In the base case (case 1), no RO_2 photolysis was considered. In this case, "virtual" sources and sinks for the longer lived species were adjusted so that their noon time concentrations maintained their initialized values at local noon. In cases 2−4, these "virtual" sources and sinks were kept the same as in the base case. Cases 2−4 included RO_2 photolysis with the above-mentioned *j* values. After a constant diurnal cycle was achieved in cases 2−4, we compared the change in the concentrations of all time-varying species from their case 1 final values. A relatively constant diurnal cycle was achieved in cases 2−4 after approximately 100 days of integration; we report the comparisons for the 198th day of the simulation. Model conditions and results from case 1 at solar noon for this day at each location are shown in Table 3.

7. Box Model Results and Discussion

The effects of including near-IR peroxyl radical photolysis on all species in the chemical mechanism depend on the competition between photolysis and the other two primary loss processes for RO_2, the reactions with NO and HO_2. We explored this competition by varying both the *j* values for RO_2 photolysis in cases 2−4 and by changing the chemical environment from remote to rural to urban. Figure 2 compares the diurnally

TABLE 3: Selected Box Model Conditions and Results from Case 1[a]

quantity	location		
	remote	rural	urban
site[b]	off SW coast of Tasmania (45°S, 144°E)	Kinterbish, Alabama (32°N, 88°W)	downtown Atlanta (34°N, 84°W)
date[b]	7 December	1 July	1 July
[M], molecule cm^{-3} [b]	2.6×10^{19}	2.4×10^{19}	2.4×10^{19}
[H_2O], %[b]	0.9	2.6	2.3
[CH_4], ppmv[b]	1.68	1.7	1.75
[OH], molecule cm^{-3}[c]	3.5×10^6	3.2×10^6	1.5×10^7
[HO_2], pptv[c]	12	38	52
[CH_3O_2], pptv[c]	10	3	8
[$CH_3CH_2O_2$], pptv[c]	0.06	0.6	10
[$HOCH_2CH_2O_2$], pptv[c]	0.02	36	9
[$CH_3C(O)O_2$], pptv[c]	0.007	0.4	2
[$HOCH_2C(O)O_2$], pptv[c,d]	0	0	0
[RO_2], pptv[c]	10	40	29
[HO_2]+[RO_2], pptv[c]	22	78	81
[H_2O_2], ppbv[e]	0.44	0.8	3.9
[CH_3OOH], ppbv[e]	0.22	0.04	0.3
[ROOH], ppbv[e]	0.003	1.1	1.0
[HCH(O)], ppbv[e]	0.12	5.7	33
[$CH_3CH(O)$], ppbv[e]	0.002	1.1	12
[$HOCH_2CH(O)$], ppbv[d,e]	0	0	0
[NO], ppbv[e]	0.006	0.2	1
[NO_2], ppbv[c]	0.008	0.9	16
[HNO_3], ppbv[e]	0.006	0.9	23
[$CH_3C(O)O_2NO_2$], ppbv[c]	0.0002	0.07	7
[$HOCH_2C(O)O_2NO_2$], ppbv[c,d]	0	0	0
[NO_y], ppbv[e]	0.020	2.1	47
[O_3], ppbv[e]	21	48	198
[CO], ppbv[e]	62	149	209
["ethane"], ppbv[e,f]	0.36	39	733
["ethene"], ppbv[e,f]	0.004	74	20

[a] Fixed and constrained quantities are average or typical values for remote (First Aerosol Characterization Experiment[36]), rural (Rural Oxidants in the Southern Environment program[27]), and urban[37] locations. ppmv = parts per million by volume, ppbv = parts per billion by volume, pptv = parts per trillion by volume. [b] Fixed. [c] Calculated value at local noon based on photochemistry only. [d] Not produced in the case 1 chemical mechanism; formed when the RO_2 photolysis reactions are allowed to occur. [e] Calculated based on photochemistry but constrained by "virtual" sources or sinks to reach this value at local noon. [f] Lumped concentration of all nonmethane alkanes or alkenes.

averaged rates of RO_2 loss via the 3 main channels at each of the locations. In any particular chemical environment, increasing the RO_2 *j* value between cases 2 and 4 dramatically changes the competition between the three loss reactions. In the rural location, HO_2 and NO reactions are more important loss terms than photolysis at the lowest RO_2 *j* values (case 2), while RO_2 photolysis predominates for the upper limit *j* values (case 4). With the increased [NO] of the rural and urban locations (Table 3), photolysis becomes less important relative to NO reaction for each individual RO_2 species. At the rural location, only the largest *j* values (case 4) give photolysis rates comparable to those of NO loss, while in the urban location, NO reaction is always the dominant loss term. However, since VOCs also increase drastically in rural and urban areas relative to remote ones (Table 3), the overall participation of larger RO_2 increases. As Figure 2 shows, the rural and urban loss rates of $CH_3CH_2O_2$, $HOCH_2CH_2O_2$ and $HOCH_2C(O)O_2$ radicals are similar to or larger than those of CH_3O_2 and much larger than their values in the remote case. This is a result of the much larger concentrations of these radicals because of higher VOC levels in the rural and urban environments (Table 3). We thus have two opposing effects in changing the chemical environment from remote to urban: photolysis of each individual RO_2 becomes less important with higher [NO] but the overall level of RO_2 increases with higher [VOCs] and somewhat offsets the effects of increasing [NO_x].

Figure 3 shows the percentage change in the diurnally averaged concentrations of a number of chemical species for each of the *j* value cases at each location. Using the lower limit RO_2 *j* values (case 2) at any of the locations, there is no significant effect of including the RO_2 photolysis reactions in the standard chemical mechanism. Methane is the major VOC in the remote environment. The levels of larger RO_2, aldehydes larger than HCH(O), and organic nitrate species are extremely small there (Table 3), so changes of a factor of 2 in their concentrations at the remote site are not significant to the overall chemistry. On the other hand, cases 3 and 4, representing midrange and upper limit RO_2 *j* values, demonstrate that RO_2 photolysis can have significant effects on some of the major species for each of the locations. In the rest of this discussion we focus on the specific changes caused by RO_2 photolysis in a few of the compounds.

[OH] increases in all chemical environments studied when peroxyl radical photolysis is included in the chemical mechanism, because [OH] is a direct product of RO_2 photolysis (R44−R47). The largest effect on diurnally averaged OH levels is seen at the rural location. Despite having higher [NO] than the remote site, the rural area's much higher VOC levels (mostly from biogenic VOCs such as isoprene) produce the highest [RO_2] and thus the greatest direct impact of the photolysis reactions of the 3 locations chosen.

HO_2 levels respond differently to RO_2 photolysis in the different locations because the controlling chemistry changes. In the remote environment, OH + CO (R9−R10) is the main source of HO_2 so that HO_2 follows the behavior of OH. In rural and urban environments, the larger VOC levels provide other sources of HO_2, such as RO_2 + NO (R20 and R23, R24−R25) and photolysis of aldehydes (R33−R34), so that HO_2 levels respond more to changes in these other species than to [OH] changes.

The levels of RO_2 species which can photolyze in the near-IR, such as CH_3O_2, $CH_3CH_2O_2$, and $HOCH_2CH_2O_2$, generally

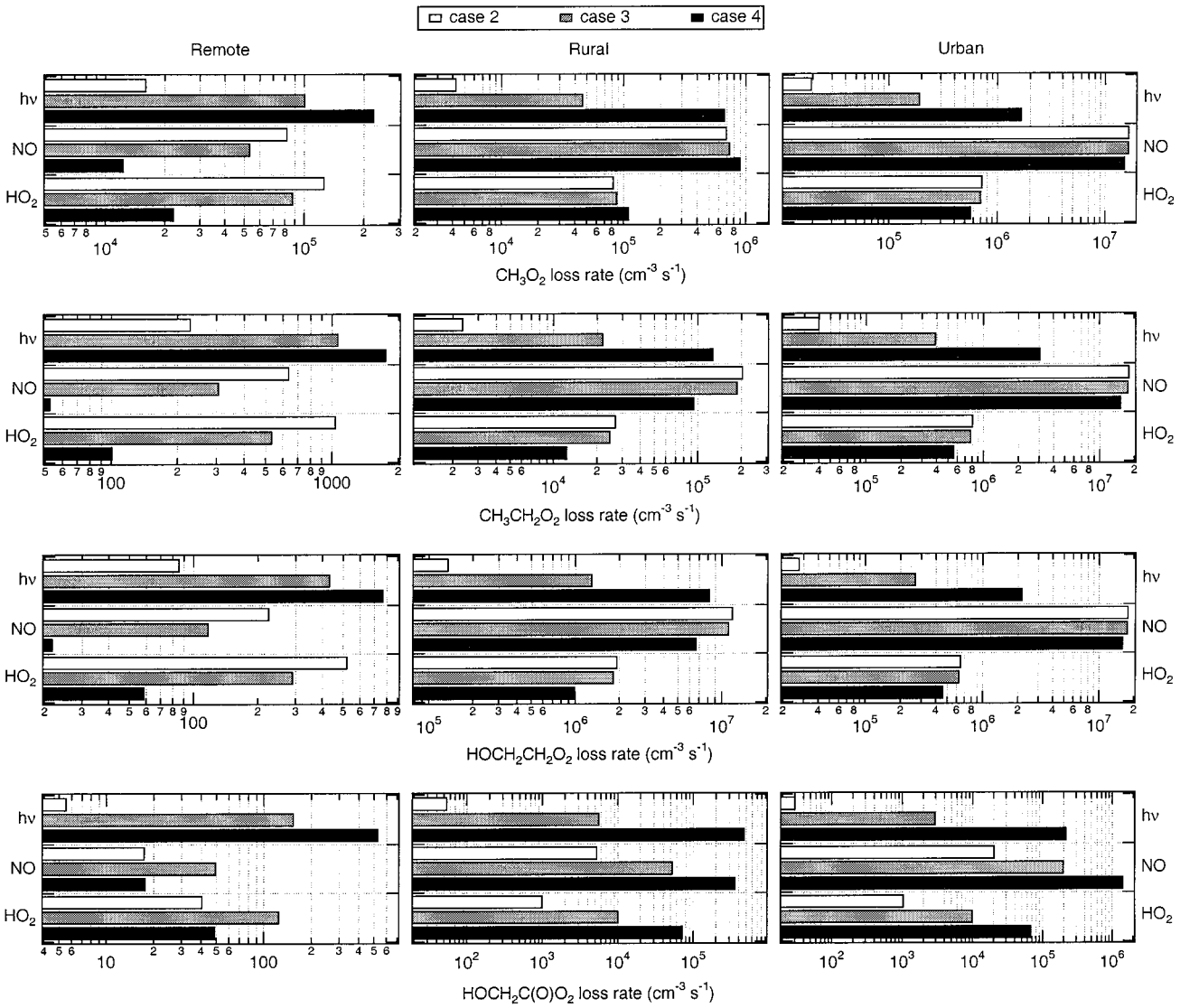

Figure 2. Diurnally averaged loss rates of selected RO_2 radicals via near-IR photolysis and reactions with NO and HO_2 for the different model locations.

decrease when this photolysis is included in the chemical mechanism because it represents an additional loss channel. Decreases in these RO_2 from the additional photolysis loss are mitigated in rural and urban areas by higher production from OH + VOCs (R11−R16). The increase in $[CH_3O_2]$ at the rural site is also due to higher $[CH_3C(O)O_2]$, which produces CH_3O_2 through self-reaction and reaction with NO.

An exception to this RO_2 behavior is HPA. Its parent molecule, HAC, is not produced in the simplified chemical mechanism considering only ethane and ethene oxidation (case 1), but only through photolysis of $HOCH_2CH_2O_2$ (R46). HAC reaches levels of up to 2 parts per billion by volume (ppbv) for the rural and urban locations, its concentration increasing with increasing $HOCH_2CH_2O_2$ *j* value. Since HPA comes only from HAC oxidation by OH, [HPA] increases with increasing $HOCH_2CH_2O_2$ *j* value even though the *j* value of HPA (and thus its loss rate) is also increasing. The concentration of HPAN also increases with increasing *j* value because of its connection to HPA through R39. Since neither HAC, HPA, or HPAN are produced in the case 1 mechanism, we cannot show their percentage changes relative to case 1 directly. Instead in Figure 3 we have grouped each of these species with its unhydroxylated cousin: HAC with $CH_3CH(O)$, represented as ∑RCH(O); HPA with PA, denoted ∑RPA; and HPAN with PAN, given by ∑RPAN. The difference between changes in these combined categories and the changes in the unhydroxylated species represent the changes in the hydroxylated compound. The increases in the ∑RPA, ∑RCH(O), and ∑RPAN categories relative to PA, $CH_3CH(O)$, and PAN show that predicted concentrations of the hydroxylated species HAC, HPA, and HPAN are significant compared with those of their unhydroxylated analogues.

Diurnally averaged concentrations of total organic peroxyl radicals, RO_2, and total peroxyl radicals, $HO_2 + RO_2$, decrease at all locations with the inclusion of RO_2 photolysis into the mechanism. In the remote environment the decrease in $[RO_2]$ is just the change in $[CH_3O_2]$ since the concentrations of other RO_2 are so small (Table 3). Decreases in $[RO_2]$ at the rural and urban locations are controlled by the decreases in $[CH_3CH_2O_2]$ and [HOCH2CH2O2], which represent the bulk of RO_2 at these sites.

Significant effects of RO_2 photolysis are seen on the levels of longer-lived compounds including peroxides, aldehydes, organic nitrates, O_3, CO, and VOCs. Changes in peroxide levels follow the behavior of $[HO_2]$ and $[RO_2]$, the peroxide precursors in R19, R21, and R26. Aldehyde concentrations at the remote location increase because they are products of RO_2 photolysis (R44−R47). At the rural and remote sites, this additional source

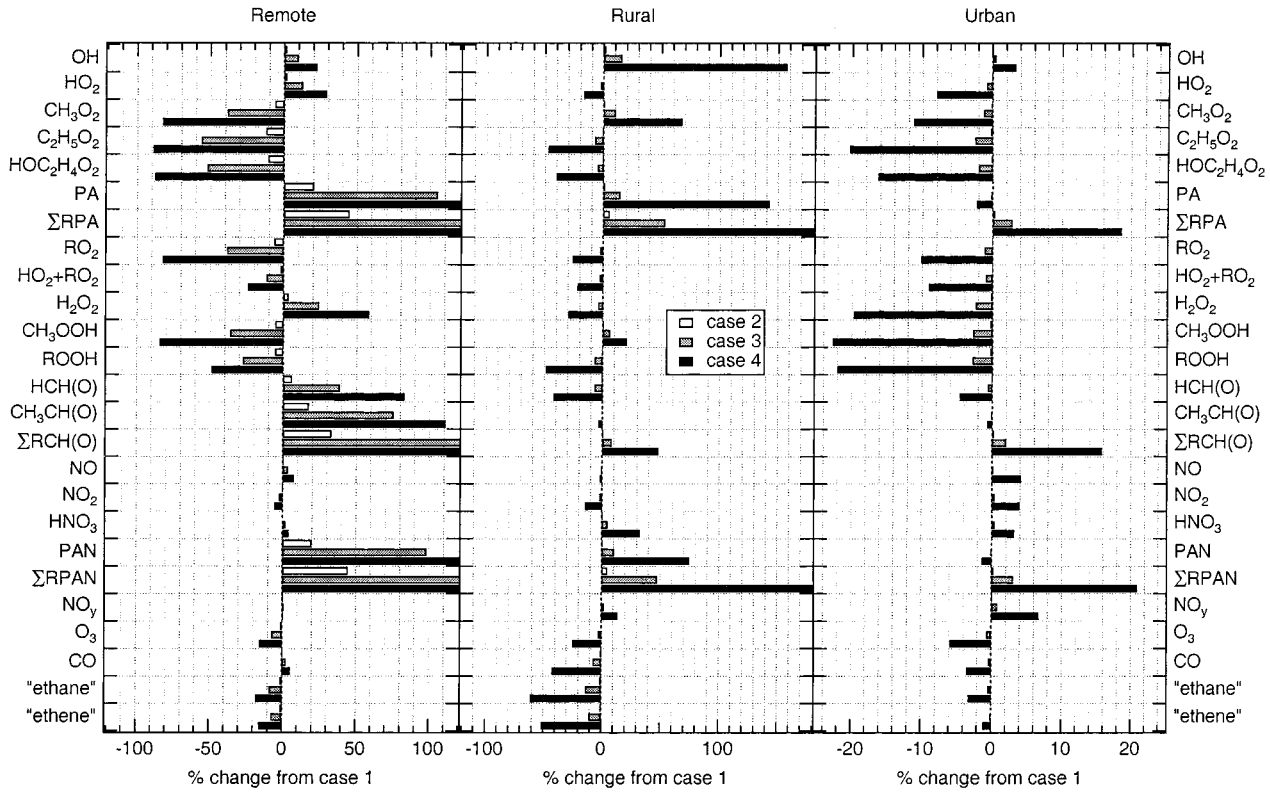

Figure 3. Percent changes in the diurnally averaged concentrations of the important model-calculated constituents when the near-IR RO_2 photolysis reactions are included.

of HCH(O) and $CH_3CH(O)$ is balanced or surpassed by increased loss due to higher [OH] (R36−R37). RO_2 photolysis changes the diurnally averaged concentrations of peroxides and aldehydes by as much as a factor of 2. Changes in the acyl peroxy nitrates reflect changes in [PA] and [HPA]. $[O_3]$ decreases at all locations, with up to a 25% diurnally averaged decrease in the rural environment. The O_3 production rate is essentially limited by the rates of HO_2 or RO_2 reactions with NO (R17, R20, R24), and changes in [NO] because of RO_2 photolysis are quite small, so that decreases in the predicted $[O_3]$ are similar to those in $[HO_2] + [RO_2]$. [CO] changes are a balance between increased sinks with OH by R9 and changing production from photolysis of HCH(O) and other aldehydes (R33−R35). At the remote site, large increases in [HCH(O)] and subsequent CO production from its photolysis dominate the small increase in [OH]. For the rural and urban locations, increases in the OH sink and decreases in the aldehyde sources work in tandem to decrease [CO] by up to 40% (case 4, rural site). VOC concentrations always decrease in the simulations carried out here because of the increasing [OH], with the largest reductions seen at the rural location.

The model response of each chemical species to RO_2 photolysis throughout the day is complex, particularly in the rural and urban cases with their more complicated chemistry. As an example, the rural location's [OH], $[HOCH_2CH_2O_2]$ (the most important RO_2 species at this location), [NO], and $[O_3]$ for cases 2−4 and their changes from case 1 as a function of time are shown in Figure 4. RO_2 photolysis changes the time response of these species somewhat, particularly for the highest j values (case 4). RO_2 photolysis has less of a zenith angle dependence than photolysis of $O_3 \rightarrow O(^1D)$ (R5) or HCH(O) (R33b) (Figure 1), because near-IR and visible wavelengths are less attenuated than ultraviolet ones in the troposphere as the zenith angle increases. Since R5 followed by R7 and R33b followed by R35 and R10 are major radical sources, we expect the greatest effect of RO_2 photolysis to occur at the largest zenith angles. [OH] shows the largest increases near sunrise and sunset, and throughout the day increases by up to 100−200% for the highest RO_2 j values. Diurnal averages of [OH] in Figure 3 show less of an increase because of the nearly negligible [OH] at night. $[HOCH_2CH_2O_2]$ decreases throughout the day and even at night although photolysis is no longer occurring, because higher nighttime [NO] results in greater $HOCH_2CH_2O_2$ loss via R24. During afternoon [NO] decreases because of faster $[NO_x]$ removal by R41. O_3 is longer lived than these other species, so the effects of RO_2 photolysis persist throughout the diurnal cycle. Decreased daytime O_3 production due to lower $[RO_2]$ causes lower $[O_3]$ throughout the entire day, including at night when no O_3 production is actually occurring.

8. Conclusions

We have investigated the tropospheric effects of a novel set of peroxyl radical photolysis reactions involving excitation from the ground electronic state to the first excited electronic state in the near-IR and subsequent rearrangement to form OH and an aldehyde. The estimated j values presume absorption cross sections which are small for an allowed electronic transition. Using cross sections more typical for such transitions, we see significant effects from these photolysis reactions on a number of species. In particular, relative to the standard chemical mechanism, we predict enhancements in OH levels, decreases in peroxyl radical levels, changes in the concentrations of the photochemical products of CO and VOC oxidation, and decreased O_3, CO, and VOC levels, with some diurnally averaged concentrations changing by as much as a factor of 2. If lower limit estimates of the near-IR j values of RO_2 are indeed correct, the diurnally averaged effects of peroxyl radical photolysis in the troposphere are probably small. Nevertheless, the chemistry described could still affect the diurnal distribution of atmospheric radicals.

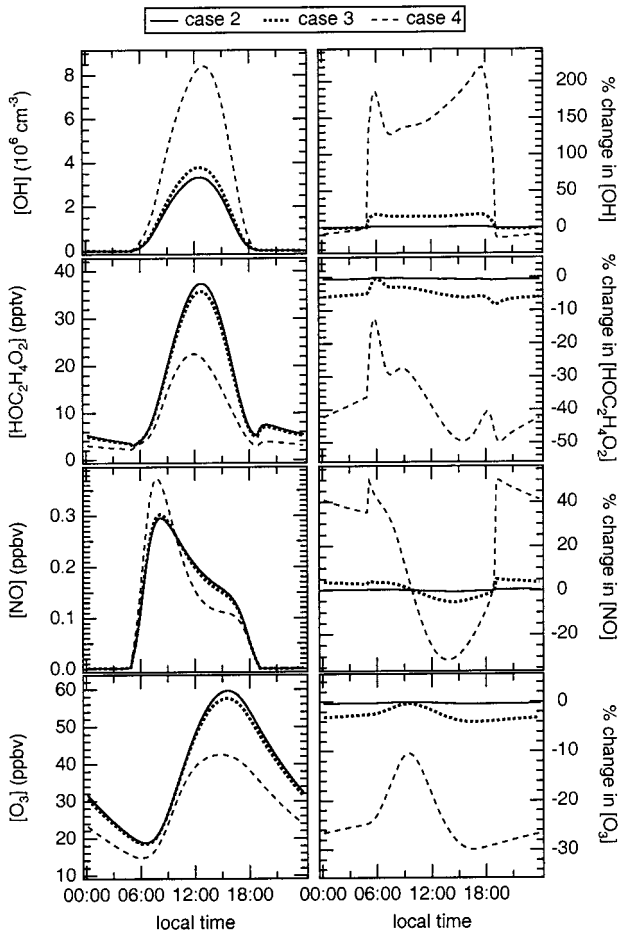

Figure 4. Concentrations of selected species for model cases 2−4 and the percent changes relative to case 1 as a function of time of day at the rural location. Case 1 concentrations of these species are indistinguishable from those of case 2 on this scale.

The presence of near-IR RO_2 photolysis in the atmosphere could be detected by looking for relationships between species which are signatures of this particular chemistry. For example, we predict that a correlation between OH and aldehyde levels should be observed at very high zenith angles as a result of RO_2 photolysis. Alternatively, one could investigate the agreement between observed levels of various chemical species and predictions from models using both the standard chemical mechanism and including RO_2 photolysis, though such an approach has its drawbacks. Model-measurement [OH] discrepancies of a factor of 2 should be detectable if the concentrations of all precursors and reactants, particularly VOCs, are measured.[7−10,29] Radical measurements are relatively new and have yet to be tested in many environments where the other necessary observations are also made. Longer-lived gases such as O_3 and CO could be measured with enough confidence[30,31] to distinguish differences of 30−50% from model predictions if chemistry were the only factor controlling their abundance. However, long tropospheric lifetimes for ozone and CO (on the order of days to months) require a three-dimensional chemical-transport model to simulate all of the various physical processes besides chemistry that have a major effect on their concentrations. The large uncertainties associated with these simulations could obscure the effects of any changes to the chemical mechanism.

The limiting uncertainties in these calculations are the absorption cross sections for the near-IR $\tilde{A} \leftarrow \tilde{X}$ transition and the yields and identities of the photoproducts. Our *j* value cases span the range of absorption cross sections for allowed electronic transitions but show drastically different results depending on the order of magnitude of these cross sections. We have used thermochemical arguments to constrain the photoproducts which are energetically accessible with near-IR excitation. Thermochemistry alone does not indicate the activation barriers or rates of various reaction paths, which must either be calculated by quantum chemical methods or, ultimately, measured in the laboratory. Experimental measurements of the absorption cross sections and photoproducts are crucial to any further understanding of the effects of the proposed chemistry. The impetus for such laboratory work is clear based on the calculations we have carried out here.

Acknowledgment. We thank the investigators from the First Aerosol Characterization Experiment for making their data available. We are indebted to Bob Portmann for his radiative transfer model results. We thank Michael Trainer and Susan Solomon for insightful discussions of this work. G.B.E. is supported by a grant from the Chemical Physics Program, United States Department of Energy (Grant DE-FG02-87ER17695). V.V. thanks the University of Colorado for a Faculty Fellowship and the National Science Foundation for continuing support.

References and Notes

(1) Lightfoot, P. D.; Cox, R. A.; Crowley, J. N.; Destriau, M.; Hayman, G. D.; Jenkin, M. E.; Moortgat, G. K.; Zabel, F. *Atmos. Environ.* **1992**, *26A*, 1805.

(2) Calvert, J. G.; Lazrus, A.; Kok, G. L.; Heikes, B. G.; Walega, J. G.; Lind, J.; Cantrell, C. A. *Nature* **1985**, *317*, 27.

(3) Thompson, A. M. *Science* **1992**, *256*, 1157.

(4) Seinfeld, J. H.; Pandis, S. N. Atmospheric Chemistry and Physics: From Air Pollution to Climate Change; John Wiley and Sons: New York, 1998.

(5) Clifford, E. P.; Wenthold, P. G.; Gareyev, R.; Lineberger, W. C.; DePuy, C. H.; Bierbaum, V. M.; Ellison, G. B. *J. Chem. Phys.* **1998**, *109*, 10293.

(6) Ehhalt, D. H. *Science* **1998**, *279*, 1002.

(7) Wennberg, P. O.; Hanisco, T. F.; Jaeglé, L.; Jacob, D. J.; Hintsa, E. J.; Lanzendorf, E. J.; Anderson, J. G.; Gao, R.-S.; Keim, E. R.; Donnelly, S. G.; Negro, L. A. D.; Fahey, D. W.; McKeen, S. A.; Salawitch, R. J.; Webster, C. R.; May, R. D.; Herman, R. L.; Proffitt, M. H.; Margitan, J. J.; Atlas, E. L.; Schauffler, S. M.; Flocke, F.; McElroy, C. T.; Bui, T. B. *Science* **1998**, *279*, 49.

(8) McKeen, S. A.; Mount, G.; Eisele, F.; Williams, E.; Harder, J.; Goldan, P.; Kuster, W.; Liu, S. C.; Baumann, K.; Tanner, D.; Fried, A.; Sewell, S.; Cantrell, C.; Shetter, R. *J. Geophys. Res.* **1997**, *102*, 6467.

(9) Eisele, F. L.; Tanner, D. J.; Cantrell, C. A.; Calvert, J. G. *J. Geophys. Res.* **1996**, *101*, 14665.

(10) Poppe, D.; Zimmerman, J.; Bauer, R.; Brauers, T.; Brüning, D.; Callies, J.; Dorn, H.-P.; Hofzumahaus, A.; Johnen, F.-J.; Khedim, A.; Koch, H.; Koppmann, R.; London, H.; Müller, K.-P.; Neuroth, R.; Plass-Dülmer, C.; Platt, U.; Rohrer, F.; Röth, E.-P.; Rudolph, J.; Schmidt, U.; Wallasch, M.; Ehhalt, D. H. *J. Geophys. Res.* **1994**, *99*, 16633.

(11) Cantrell, C. A.; Lind, J. A.; Shetter, R. E.; Calvert, J. G.; Goldan, P. D.; Kuster, W.; Fehsenfeld, F. C.; Montzka, S. A.; Parrish, D. D.; Williams, E. J.; Buhr, M. P.; Westberg, H. H.; Allwine, G.; Martin, R. *J. Geophys. Res.* **1992**, *97*, 20.

(12) Hunziker, H. E.; Wendt, H. R. *J. Chem. Phys.* **1976**, *64*, 3488.

(13) Lightfoot, P. D.; Roussel, P.; Veyret, B.; Lesclaux, R. *J. Chem. Soc., Faraday Trans.* **1990**, *86*, 2927.

(14) Ravishankara, A. R. *Annu. Rev. Phys. Chem.* **1988**, *39*, 367.

(15) Goddard, W. A., III.; Harding, L. B. *Annu. Rev. Phys. Chem.* **1978**, *29*, 363.

(16) Petersson, G. A. 1999. Personal communication.

(17) Pilling, M. J.; Robertson, S. H.; Seakins, P. W. *J. Chem. Soc., Faraday Trans.* **1995**, *91*, 4179.

(18) Baldwin, R. R.; Dean, C. E.; Walker, R. W. *J. Chem. Soc., Faraday Trans. 2* **1986**, *82*, 1445.

(19) Wagner, A. F.; Slagle, I. R.; Sarzynski, D.; Gutman, D. *J. Phys. Chem.* **1990**, *94*, 1853.

(20) Walch, S. P. *Chem. Phys. Lett.* **1993**, *215*, 81.

(21) Quelch, G. E.; Gallo, M. M.; Schaefer, H. F., III. *J. Am. Chem. Soc.* **1992**, *114*, 8239.

(22) Quelch, G. E.; Gallo, M. M.; Shen, M.; Xie, Y.; Schaefer, H. F., III.; Moncrieff, D. *J. Am. Chem. Soc.* **1994**, *116*, 4953.
(23) Madronich, S. TUV−Tropospheric ultraviolet and visible model. Technical note; National Center for Atmospheric Research. In preparation.
(24) Hunziker, H. E.; Wendt, H. R. *J. Chem. Phys.* **1974**, *60*, 4622.
(25) Portmann, B. 1999. Personal communication.
(26) Okabe, H. Photochemistry of Small Molecules; John Wiley and Sons: New York, 1978.
(27) Frost, G. J.; Trainer, M.; Allwine, G.; Buhr, M. P.; Calvert, J. G.; Cantrell, C. A.; Fehsenfeld, F. C.; Goldan, P. D.; Herwehe, J.; Hübler, G.; Kuster, W. C.; Martin, R.; McMillen, R. T.; Montzka, S. A.; Norton, R. B.; Parrish, D. D.; Ridley, B. A.; Shetter, R. E.; Walega, J. G.; Watkins, B. A.; Westberg, H. H.; Williams, E. J. *J. Geophys. Res.* **1998**, *103*, 22491.
(28) DeMore, W. B.; Sander, S. P.; Golden, D. M.; Hampson, R. F.; Kurylo, M. J.; Howard, C. J.; Ravishankara, A. R.; Kolb, C. E.; Molina, M. J. Chemical kinetics and photochemical data for use in stratospheric modeling, evaluation no. 12. Publication 97−4; NASA/Jet Propulsion Laboratory: Pasadena, California, 1997.
(29) Mauldin, R. L.; Madronich, S.; Flocke, S. J.; Eisele, F. L.; Frost, G. J.; Prevot, A. S. H. *Geophys. Res. Lett.* **1997**, *24*, 3033.
(30) Parrish, D. D.; Trainer, M.; Williams, E. J.; Fahey, D. W.; Hübler, G.; Eubank, C. S.; Liu, S. C.; Murphy, P. C.; Albritton, D. L.; Fehsenfeld, F. C. *J. Geophys. Res.* **1986**, *91*, 5361.
(31) Parrish, D. D.; Trainer, M.; Buhr, M. P.; Watkins, B. A.; Fehsenfeld, F. C. *J. Geophys. Res.* **1991**, 96.
(32) Chen, J.; Young, V.; Hooshiyar, P. A.; Niki, H.; Hurley, M. D. *J. Phys. Chem.* **1995**, *99*, 4071.
(33) Turecek, F.; Havlas, Z. *J. Org. Chem.* **1986**, *51*, 4066.
(34) Holmes, J. L.; Lossing, F. P. *J. Am. Chem. Soc.* **1982**, *104*, 2648.
(35) Rossi, M.; Golden, D. M. *Int. J. Chem. Kinet.* **1979**, *11*, 715.
(36) Bates, T. S.; Huebert, B. J.; Gras, J. L.; Griffiths, F. B.; Durkee, P. A. *J. Geophys. Res.* **1998**, *103*, 16297.
(37) Chameides, W. L.; Fehsenfeld, F.; Rodgers, M. O.; Cardelino, C.; Martinez, J.; Parrish, D.; Lonneman, W.; Lawson, D. R.; Rasmussen, R. A.; Zimmerman, P.; Greenberg, J.; Middleton, P.; Wang, T. *J. Geophys. Res.* **1992**, *97*, 6037.